

Supporting Information

Experiment Section

Materials

Glycerol tripalmitate, sodium cholate, doxorubicin hydrochloride, soybean lecithin (L- α -Phosphatidylcholine), nystatin, chlorpromazine, cytochalasin D, nocodazole, phosphotungstic acid, methylthiazolotetrazolium, dimethyl sulfoxide, paraformaldehyde, porcine pancreatic lipase, colipase from porcine pancreas and Cyclosporin A (Cys A) were purchased from the Sigma-Aldrich Chemical Co. (USA). Non-esterified free acid (NEFA) assay kit was purchased from Wako Diagnostics (USA). All chemicals and solvents were of analytical reagent grade.

Preparation of D-PL RMs, D-PL/TG NPs and triglyceride nanoparticles

One milligram of doxorubicin hydrochloride was dissolved in deionized water with various weights of CHC (weight ratio 10% and 30%), and the pH value of these solution were adjusted to 8.0 (above isoelectric point of CHC, approximately 6.2) to ensure the CHC with negative charges. Glycerol tripalmitate (0.5% w/v) and lecithin were dissolved in chloroform. The DOX solutions were subsequently mixed with the chloroform solutions and the D-PL RMs were obtained after emulsifying the mixtures at 40 W using an ultrasonic processor (Hielscher, Germany).

The prepared D-PL RMs (CHC ratio in the reverse micelles varied from 0% to 40%) were then added into 1% w/v sodium cholate aqueous solutions and followed by emulsifying again at 100 W to form w/o/w solution. After removing the organic solvent using a rotary vacuum evaporator (Eyela, Japan), the D-PL/TG NPs were precipitated and redispersed in aqueous solution. To remove the excess surfactants and un-encapsulated drugs, the D-PL/TG NPs were washed three times by centrifuging at 8000 rpm and were resuspended in deionized water. The reverse micelles- and DOX-free triglyceride nanoparticles (TNPs) were also prepared by

similar synthesis procedure. Glycerol tripalmitate (GT) was dissolved in chloroform (0.5% w/v) and were mixed with an aqueous phase containing sodium cholate (1% w/v). The solution was emulsified at 100 W and then followed by removing the organic solvent to obtain TNPs in aqueous solution. To remove the excess surfactants, the TNPs were washed by centrifuging three times at 8000 rpm and subsequently resuspended in deionized water.

Characterization of D-PL RMs and D-PL/TG NPs

Pure CHC and lecithin were dissolved in deionized water (1% w/v) and chloroform (10 mg mL⁻¹), respectively. Then 20 µL of the samples were dropped on KBr pellets and dried at room temperature. FTIR spectra were recorded with KBr pellets on a Perkin-Elmer spectrum 100 (USA) in the spectral region (4000–450 cm⁻¹) with 64 scans recorded at a resolution of 4 cm⁻¹. The morphology of the D-PL RMs and D-PL/TG NPs was observed by transmission electron microscopy (TEM) (JEM-2100F, Japan). The prepared method of TEM samples for the D-PL RMs were modified from the previous study.¹ Briefly, phosphotungstic acid (PTA) was added into the solution of DOX and CHC (final concentration 2 %) and the D-PL RMs was prepared according to the standard procedure. A droplet of the prepared D-PL RMs was dropped on a Lacey Cu grid and dried at room temperature. The TEM sample of the D-PL/TG NPs was negatively stained by 2% PTA solution after they were precipitated and then dropped on a Lacey Cu grid to be dried at room temperature.

The average size and zeta potential of the D-PL/TG NPs were measured by dynamic light scattering (Delsa Nano C, Beckman Coulter, USA). 500 µL of the D-PL/TG NPs were loaded in a quartz cell and measured under an incident light (particle size) or electric field (zeta potential). All experiments were performed in triplicate. Samples of the D-PL/TG NPs for X-ray diffraction (XRD), differential scanning calorimetry (DSC) and small angle X-ray scattering (SAXS) were frozen

and dried in a freeze-dryer (Labconco Corp., USA) for 48 h before analysis. XRD studies were performed on the D8 Discover (Bruker Corp., Germany) by exposing the samples to CuK α radiation (30 kV, 10 mA) and scanned from 7.5° to 70°, 2h at a step size of 0.045° and step time of 0.5 s. DSC measurements were performed using a Diamond DSC (Perkin-Elmer Corp., USA). A heating rate of 10 °C min⁻¹ was employed in the temperature range of 40–85 °C. An empty aluminum pan was used as the reference standard. Analysis was carried out under a purge of nitrogen gas. SAXS studies were performed on a Bede D1 system with Cu K α radiation ($\lambda = 0.154\ 06\ \text{nm}$, 1.0° ~ 5.0°).

Drug encapsulation efficiency

1 mL of the D-PL/TG NPs solution (10 mg mL⁻¹) was centrifuged at 8000 rpm, and the supernatant was collected. The quantity of un-encapsulated DOX was determined using ultraviolet (UV) absorption at a wavelength of 480 nm, a strong absorption band of DOX, with reference to a calibration curve on a UV-Vis spectrometer (Agilent, 84531 UV-Visible spectrophotometer). Encapsulation efficiency (EE) was determined using the following equation:

$$EE = [(W_i - W_f) / W_i] \times 100 \%$$

where W_i is the initial amount of DOX, and W_f is the amount of un-encapsulated DOX in the supernatant.

In vitro release study

To determine the release profile of the D-PL/TG NPs, the solution (10 mg mL⁻¹) was added into a dialysis tubing cellulose membrane with a cutoff molecular weight of 12,000. The dialysis bags were dialyzed in phosphate buffer (pH 7.4) at 37 °C with gentle shaking, and aliquots of incubation medium were removed at predetermined time points. The amounts of released drugs were quantified using UV-Vis spectrometer. The solution was maintained at a constant volume by replacing original

solution with fresh media. All experiments were performed in triplicate.

Kinetic studies of triglyceride degradation by lysosomal acid lipase and DOX

release

Lysosomal acid lipase (LAL)-mediated degradation assay was performed based on a previously described method.^{2, 3} Briefly, lipase and colipase were dissolved in distilled water at concentrations of 2000 U mL⁻¹ lipase and 50 µg mL⁻¹ colipase. The mixture of 600 µL lipase solution and 360 µL of colipase solution were incubated at 37 °C for 15 min to form the lipase/colipase complex and then reconstituted using citrate buffer (0.1 M) at pH4.8, the pH value of lysosomal content. 200 µL suspension containing 10 mg drug-free PL/TG NPs was added to 2300 µL LAL suspension at 37 °C with magnetic stirring to initiate the degradation reaction. At predetermined time points, 50 µL aliquots of the mixture were drawn and analyzed using NEFA assay kit. Colorimetric changes related to concentrations of free fatty acids were measured using Sunrise absorbance microplate reader at 550 nm with oleic acid (OA) as a standard. The fatty acids released from the lipid nanoparticles were quantified and expressed in terms of the percentage of fatty acids that can possibly be freed after complete degradation. The release of the entrapped OA and formation of free fatty acids from LAL enzymatic degradation of the triglyceride components were all included,⁴ and the experiments were performed in triplicate.

A release kinetics study of the encapsulated DOX from D-PL/TG NPs was performed using a modified experimental procedure. The mixture of 200 µL suspension containing 10 mg D-PL/TG NPs and 2300 µL LAL suspension was added to a dialysis tubing cellulose membrane with a cutoff molecular weight of 12,000. The dialysis bags were dialyzed in phosphate buffer (pH 7.4) at 37 °C with gentle shaking, and aliquots of incubation medium were removed at predetermined time points. The amounts of released drugs were quantified using UV-Vis spectrometer. The solution

was maintained at a constant volume by replacing original solution with fresh media. All experiments were performed in triplicate.

Mechanism of endocytosis

MCF-7 human breast carcinoma cells were grown in 75T culture flasks in DMEM culture medium supplemented with 10% FBS and 1% penicillin–streptomycin–neomycin solution at 37 °C under 5% CO₂ and sub-cultured 2~3 times per week with 0.25% trypsin–EDTA. To investigate the endocytic mechanism related to internalization of the D-PL/TG NPs, the cells were cultured in a 6-cm dish at a density of 10⁶ per dish for 24 h and followed by incubating for 60 min with 10 μM nystatin (inhibitor of caveolae-mediated endocytosis), 10 μg mL⁻¹ chlorpromazine (inhibitor of clathrin-mediated endocytosis) or 3 μM cytochalasin D (inhibitor of macropinocytosis), prior to 4 h of incubation with D-PL/TG NPs. The fluorescence was measured by flow cytometer (FACSCalibur, USA), and the experiments were performed in triplicate.

Subcellular localization of D-PL/TG NPs

MCF-7 cells were seeded on 22-mm² glass coverslips placed in 6-well plates. After incubation for 12 h, the cells were stained by CellLight Lysosomes-GFP (Molecular Probes Inc., USA) and incubated for an additional 24 h. D-PL/TG NPs were added into each well at a concentration of 20 μg mL⁻¹. After 4 h, the cells were harvested and washed several times with PBS. The cells were later fixed with 3.7% paraformaldehyde solution and stained by DAPI. Subcellular localization was visualized using confocal laser scanning microscope (CLSM, D-Eclipse C1, Nikon, USA).

Assays of cellular cytotoxicity and uptake

In vitro cytotoxicity of free DOX solution and D-PL/TG NPs were examined on MCF-7 cells and MCF-7/ADR cells using methylthiazoletetrazolium (MTT) method.

DOX-resistant (MCF-7/ADR) human breast carcinoma cells were kindly provided by Professor Ming-Jium Shieh (National Taiwan University, Taiwan) and grown in 75T culture flasks in DMEM culture medium supplemented with 10% FBS and 1% penicillin–streptomycin–neomycin solution at 37 °C under 5% CO₂. The cells were continuously maintained in 0.5 μM DOX. In viability assay, 1 × 10⁴ cells/well were plated in 96-well plates and exposed to serial concentrations of equivalent DOX at 37 °C for 72 h. Subsequently, 20 μL of MTT solution (5 mg mL⁻¹ in PBS, pH 7.4) was added, and the cells were incubated for an additional 4 h. Subsequently, the medium was replaced with 200 μL of dimethyl sulfoxide (DMSO), and the absorbance was monitored using a Sunrise absorbance microplate reader at the wavelength of 595 nm. Finally, the cell viability was determined by comparison with untreated control and calculated using the following equation:

$$\text{Cell Viability (\%)} = (A_{\text{sample}} / A_{\text{control}}) \times 100\%$$

The half maximal inhibitory concentration (IC₅₀), which is defined as the dosage of a compound that inhibited 50% of cell growth, was calculated from the obtained viability curves.

The amount of free DOX, free DOX mixed with Cys A, or D-PL/TG NPs uptaken by MCF-7/ADR cells was detected using flow cytometer. The cells were seeded in 6 cm dish at a density of 10⁶ per dish and incubated for 24 h before use. Equivalent amounts of DOX (10 μg mL⁻¹) were added and incubated with the cells. After incubation for 4 h, the cells were harvested to measure the DOX fluorescence. The fluorescence was measured using flow cytometer. All experiments were performed in triplicate.

Statistical analysis

All of the results were expressed as the mean \pm standard deviation (SD). Statistical tests were performed using Excel (Version 2010, Microsoft) with two-tailed Student's t test. P values less than 0.05 were considered to be statistically significant.

Figures

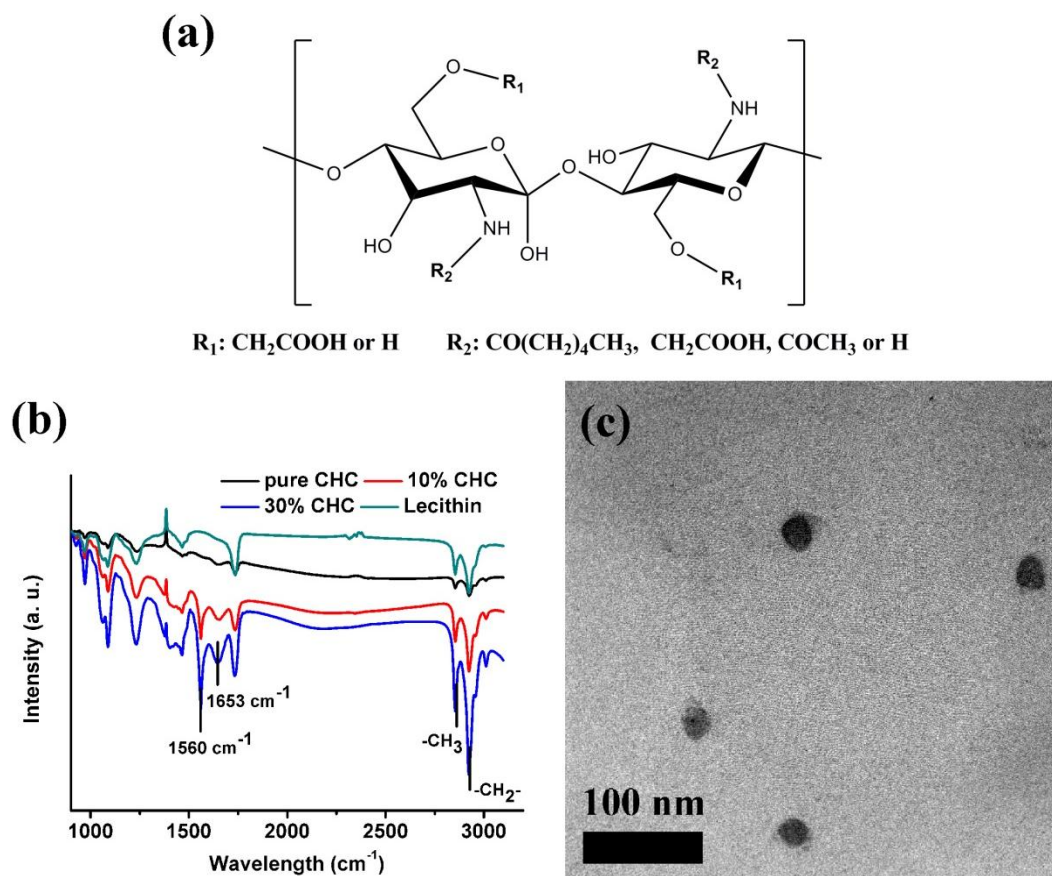


Figure S1. (a) Chemical structure of CHC. The amphiphilic CHC was chemically modified pristine chitosan with nearly 50% of hydroxyl groups substituted by carboxymethyl ligand and 48% of amine groups replaced with hydrophobic hexanoyl groups. (b) The normalized FTIR spectra of pure CHC, lecithin, and the D-PL RMs with 10% and 30% CHC compositions. (c) TEM image of D-PL RMs with 30% CHC. In previous work⁵, the FTIR spectra in Figure S1b shows the absorption peaks from hydrophobic functional groups of CHC at ca. 1560 cm^{-1} to the N-H bending vibrations of the amide II band, at 1653 cm^{-1} to the carbonyl stretching of secondary amides (amide I band), and at $2850\text{--}2930 \text{ cm}^{-1}$ to the stretching of $-\text{CH}_3$ and $-\text{CH}_2-$. In this study, the results clearly illustrate an increased intensity of the absorption peaks at 1560 cm^{-1} , 1653 cm^{-1} , and $2850\text{--}2930 \text{ cm}^{-1}$. According to the previous observation,

associated with the w/o emulsification process designed in this first stage of synthesis, it is rationally to depict that those hydrophobic phase extended outside the RMs showed stronger signal, and became more pronounced with increasing CHC. In the meantime, upon increasing CHC, its hydrophilic segments should provide better chemical affinity toward the DOX, resulting in higher drug encapsulation efficiency as observed experimentally.

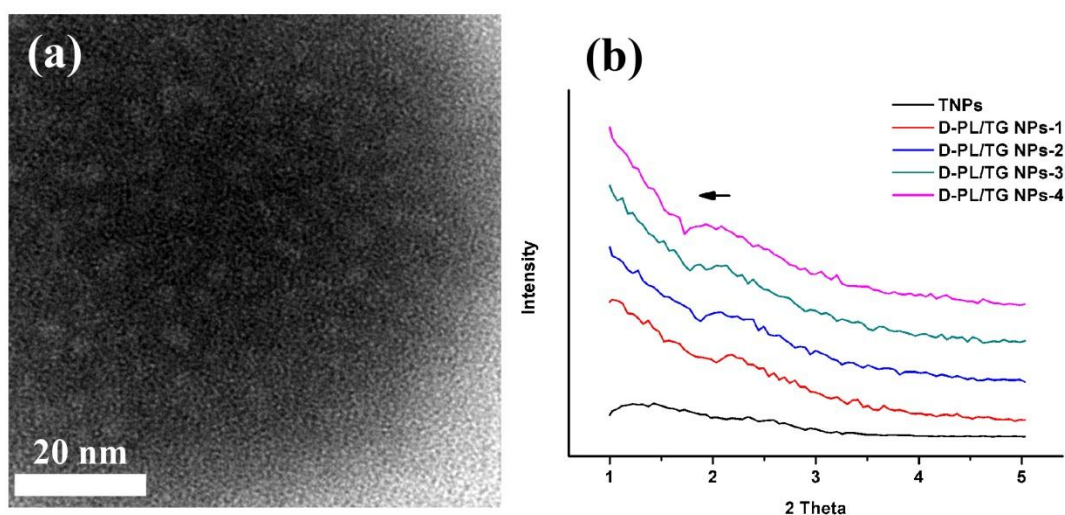


Figure S2. (a) Localized region under high magnification of D-PL/TG NPs with 10% by transmission electron microscopy. (b) Diffraction patterns of designed D-PL/TG NPs (described in Table S1) and TNPs were analyzed by SAXS with Cu K α radiation ($\lambda = 0.154\ 06\ \text{nm}$, $1.0^\circ \sim 5.0^\circ$). The mean diameter of the pores is approximately 4 nm for D-PL/TG NPs with 10% CHC (Fig. S2a), but it increases to 8 nm for D-PL/TG NPs with 30% CHC (Fig. 1d), suggesting an effect of CHC, where a larger polysaccharide-lecithin reverse micelles evolved as the CHC ratio is increased. The TEM image of D-PL RMs with 30% CHC shows that the mean diameter was about 20 nm. It seems that while the aqueous phase was removed completely from the core phase, giving a nanocavity evolved in the RMs with a size of about 8 nm due to collapse of the reverse micelles. SAXS was employed to characterize porous structure of the nanoparticles by examining the spectral deviation as a result of variations in pore structure within the D-PL/TG NPs. Figure S2b shows that the spectral peaks of the D-PL/TG NPs with various CHC ratio are shifted to lower diffraction angles, suggesting an increasing CHC ratio causes an increase in pore size.⁶ At low CHC ratio, the reverse micelle was composed of a small number of CHC molecules with a small population of negatively charged functional groups residing at the interface between organic solvent and water. Under this configuration, weaker intramolecular and

intermolecular repulsion resulted in reduced micellular size. In contrast, at high CHC ratio, a greater amount of CHC molecules aggregated to form the reverse micelle. The resulting electrostatic repulsions originating from the negatively charged functional groups on both lecithin and CHC became stronger, leading to a larger micellular size and particle size, which was consistent with TEM examinations and dynamic light scattering measurements.

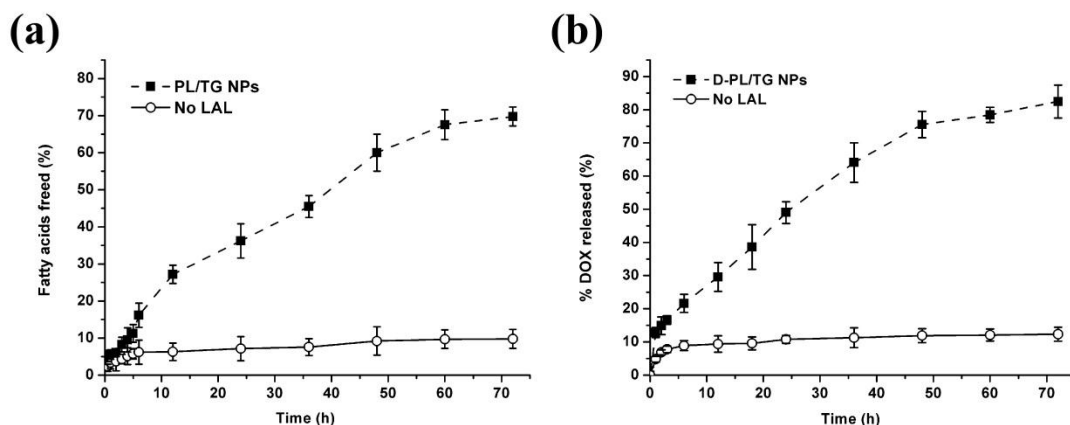


Figure S3. The amount of free fatty acids released in response to LAL activity was measured to quantify the degradation level of the PL/TG NPs. (a) The degradation profiles of PL/TG NPs at 37 °C under presence and absence (no LAL) of lysosomal acid lipase (LAL) buffer. Time changes in the free fatty acids formed from triglyceride degradation and release of entrapped oleic acid were measured in triplicate. The results reveal that less than 10 % degradation of PL/TG NPs occurred in the absence of LAL for 72 h, whereas 70% degradation of PL/TG NPs occurred under the action of LAL. (b) The DOX release profiles at 37 °C under presence and absence (no LAL) were presented. The experiments were performed in triplicate. The results show that more than 80% of encapsulated DOX was released in the presence of LAL, but only 12% of encapsulated DOX was released without LAL.

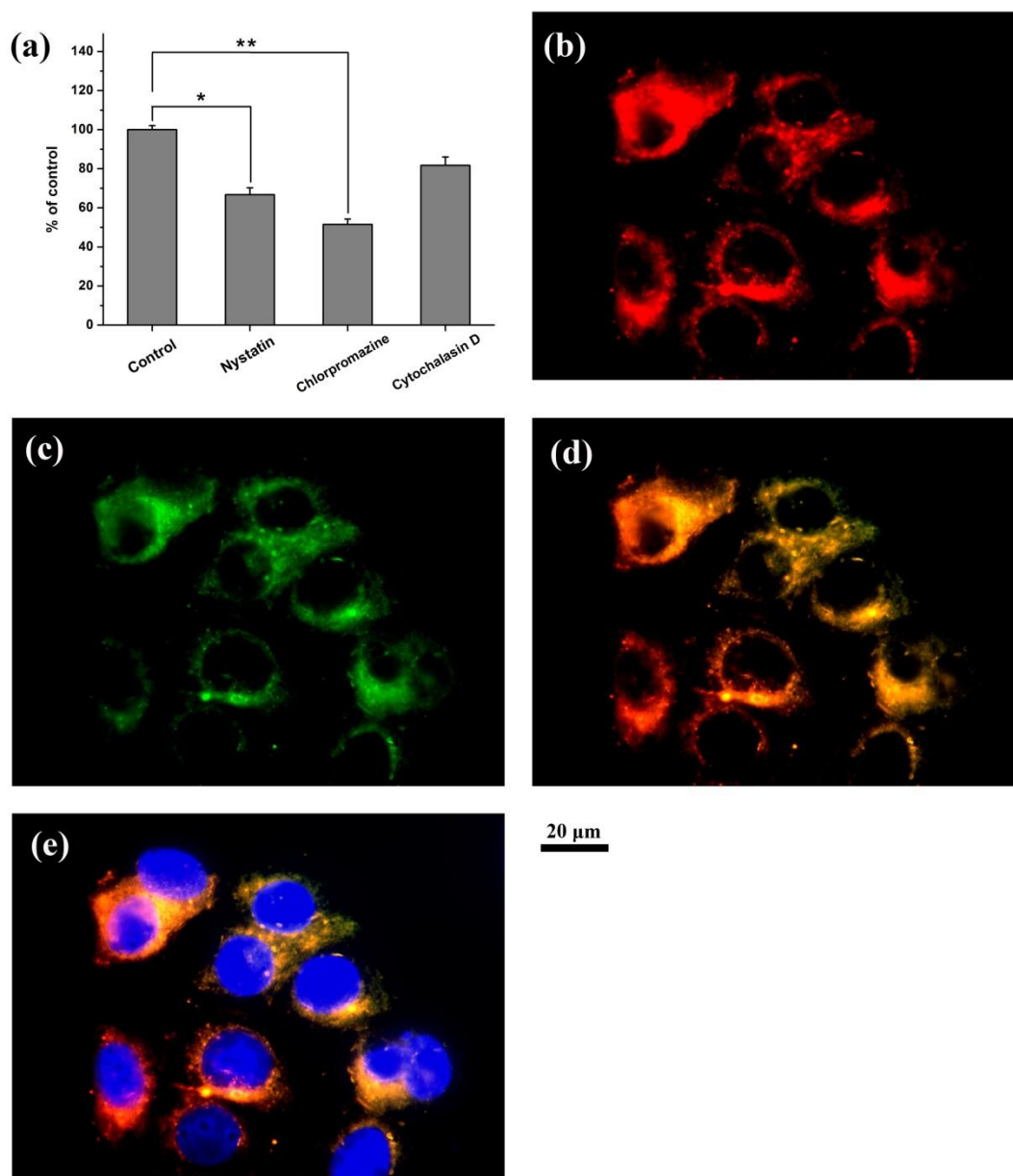


Figure S4. (a) Evaluation of D-PL/TG NPs uptake by MCF-7 cells after incubated with nystatin, chlorpromazine and cytochalasin D at 37 °C vs. control (no inhibitor treatment) at 37 °C. The fluorescent intensity of MCF-7 cells was detected by flow cytometry. $**p < 0.01$ and $*p < 0.05$ compared to control group. Fluorescent images of MCF-7 cells after treatment with D-PL/TG NPs for fluorescence labeling experiments: (b) D-PL/TG NPs (c), lysosomes, (d) colocalization of (b) and (c) fluorescence, and merged (d) with DAPI (e). To examine the endocytic pathway of D-PL/TG NPs, we incubated MCF-7 cells with several specific endocytic inhibitors and measured their fluorescence intensity. As shown in Fig. S4a, the cells incubated with chlorpromazine or nystatin exhibited lower fluorescence intensity (49% and 34%, respectively) compared to control group. The results indicate that the internalization

of D-PL/TG NPs was likely a mixed model of clathrin and caveolae-mediated endocytosis (inhibited by chlorpromazine and nystatin, respectively), and the former, i.e., clathrin-mediated endocytosis, appeared to be the dominating pathway. Namely, nanoparticles were most likely internalized by clathrin-coated vesicle to traffic through the cell, and the vesicle subsequently matured into early and late endosomes, which is known as endolysosomal pathway.⁷ The endosomes finally led to fusion with lysosomes, in which the internalized nanoparticles are degraded by lysosomal enzymes.

Confocal microscopy was used to visualize the subcellular localization of the internalized nanoparticles. Figure S4b reveals that majority of D-PL/TG NPs are localized in cytoplasm region after 4-h incubation. To identify the cellular distribution more clearly, we executed double-labeling experiments and visualized the red fluorescence from DOX, blue fluorescence from DAPI (specific for nucleus) and green fluorescence from CellLight Lysosomes-GFP (specific for lysosomes, Fig. S5c). By colocalizing the red and green fluorescence signals (Fig. S5d), it was evidenced that the D-PL/TG NPs were localized within lysosomes. These results confirm that D-PL/TG NPs were delivered into lysosomes and subsequently the triglyceride shell was degraded by LAL to release the drug intracellularly.

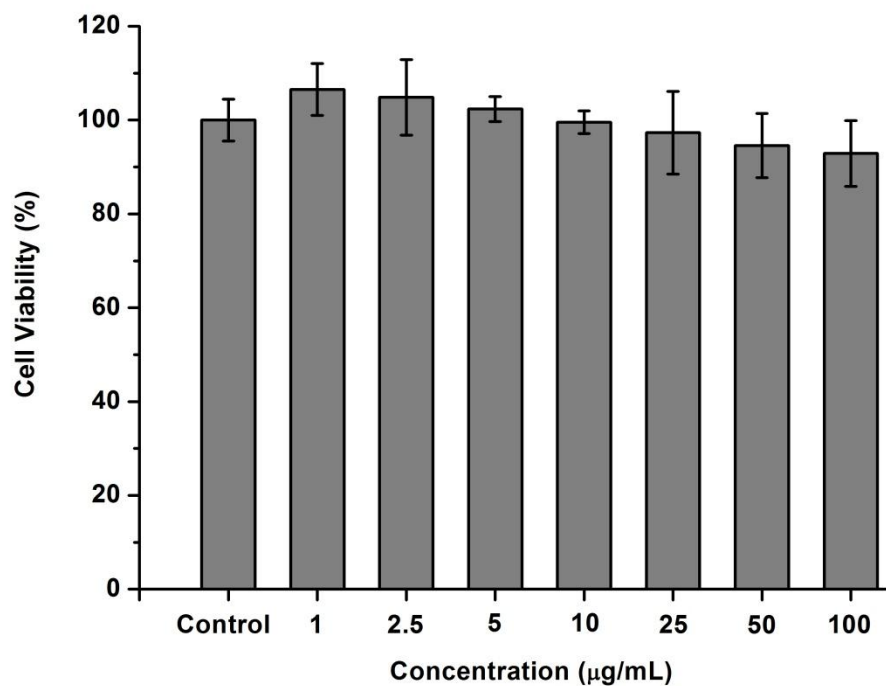


Figure S5. In vitro cytotoxicity of drug-free PL/TG NPs with different concentrations against MCF-7 cells for 24 h treatment. All experiments were performed in triplicate. The results indicate that the feeding amount of drug-free PL/TG NPs was non-cytotoxic and well biocompatible for MCF-7 cells. In the MTT test of D-PL/TG NPs against MCF-7 cells and MCF-7/ADR cells, the feeding amount of carriers were all under $100 \mu\text{g mL}^{-1}$.

Tables

Sample	Ratio of CHC in the reverse micelles (% w/w)	Mean diameter (nm)	Polydispersity index	Zeta potential (mV)
D-PL/TG NPs -0	0	161.7±4.1	0.225±0.018	-33.5±0.42
D-PL/TG NPs -1	10	169.5±5.2	0.238±0.008	-29.21±0.56
D-PL/TG NPs -2	20	175.3±3.6	0.123±0.030	-30.70±0.48
D-PL/TG NPs -3	30	178.3±4.1	0.214±0.030	-31.54±1.02
D-PL/TG NPs -4	40	181.4±5.5	0.223±0.054	-29.35±1.83

Table S1. Mean diameter, PDI, and zeta potential of the D-PL/TG NPs.

	Melting peak (°C)	Enthalpy (J/g)	Onset (°C)	Maximum (°C)
GT	64.60	214.19	57.68	67.05
TNPs	61.63	138.47	54.29	63.99
PL/TG NPs	58.23	58.90	54.06	61.09
D-PL/TG NPs	55.17	42.58	53.92	60.26

Table S2. Melting peaks, enthalpy, onset and maximum temperature of GT, TNPs, PL/TG NPs and D-PL/TG NPs.

Reference

1. H. M. Jung, K. E. Price and D. T. McQuade, *Journal of the American Chemical Society*, 2003, **125**, 5351-5355.
2. C. Olbrich, O. Kayser and R. H. Muller, *Int. J. Pharm.*, 2002, **237**, 119-128.
3. H. Y. Xue and H. L. Wong, *Biomaterials*, 2011, **32**, 2662-2672.
4. P. Nilssonhle, A. S. Garfinkel and M. C. Schotz, *Annu. Rev. Biochem*, 1980, **49**, 667-693.
5. K. H. Liu, B. R. Chen, S. Y. Chen and D. M. Liu, *J. Phys. Chem. B*, 2009, **113**, 11800-11807.
6. Z. Konya, V. F. Puentes, I. Kiricsi, J. Zhu, A. P. Alivisatos and G. A. Somorjai, *Nano Lett.*, 2002, **2**, 907-910.
7. L. A. Bareford and P. W. Swaan, *Adv. Drug Del. Rev.*, 2007, **59**, 748-758.